Check for updates

View Article Online
View Journal

PCCP
Physical Chemistry Chemical Physics

Accepted Manuscript

This article can be cited before page numbers have been issued, to do this please use: J. Sun, Z. Fu, J. Zhang, Z. Tao, M. Wang and C. Zhou, *Phys. Chem. Chem. Phys.*, 2026, DOI: 10.1039/D5CP04721H.

This is an Accepted Manuscript, which has been through the Royal Society of Chemistry peer review process and has been accepted for publication.

Accepted Manuscripts are published online shortly after acceptance, before technical editing, formatting and proof reading. Using this free service, authors can make their results available to the community, in citable form, before we publish the edited article. We will replace this Accepted Manuscript with the edited and formatted Advance Article as soon as it is available.

You can find more information about Accepted Manuscripts in the Information for Authors.

Please note that technical editing may introduce minor changes to the text and/or graphics, which may alter content. The journal's standard Terms & Conditions and the Ethical guidelines still apply. In no event shall the Royal Society of Chemistry be held responsible for any errors or omissions in this Accepted Manuscript or any consequences arising from the use of any information it contains.

ROYAL SOCIETY OF CHEMISTRY

rsc.li/pccp

View Article Online
DOI: 10.1039/D5CP04721H

Open Access Article. Published on 02 June 2026. Downloaded on 6/3/2026 5:39:24 AM.
This article is licensed under a Creative Commons Attribution 3.0 Unported Licence.

Physical Chemistry Chemical Physics Accepted Manuscript

Multi-Structural Kinetics Study on H-atom Abstraction from Fuel Molecules by $\dot{N}H_2$ Radicals with Anharmonicity, Recrossing and Tunneling Effects

Jingwu Sun[a, b1], Zhaolin Fu[c1], Junyue Zhang[a], Zhiping Tao[c], Mengyuan Wang[a*], Chong-Wen Zhou[a,d*]

[a] *School of Energy and Power Engineering, Beihang University, Beijing 100191, PR China*
[b] *National Institute of Clean-and-Low-carbon Energy, Beijing, 102211, China.*
[c] *Research Institute of Petroleum Processing, Sinopec, 18 Xueyuan Road, Haidian District, Beijing 100083, PR China*
[d] *Combustion Chemistry Centre, School of Biological and Chemical Sciences, MaREI, Ryan Institute, University of Galway, alway H91TK33, Ireland*
[1] *These authors contributed equally.*

Email: mengyuanwang@buaa.edu.cn; chongwen.zhou@universityofgalway.ie

Abstract
Hydrogen atom abstraction (HAA) reactions by $\dot{N}H_2$ radicals from fuel molecules are critical in ammonia combustion chemistry, particularly in the co-combustion of ammonia with high reactivity fuels, as these C–N cross-reactions play a pivotal role in the development of ammonia blend fuel mechanisms. This study explored the influence of multi-structural effects on the kinetics and thermodynamics of HAA reactions from a range of representative alkanes (*n*-butane, *iso*-butane, *n*-pentane, *iso*-pentane, *n*-heptane, and *iso*-octane) and oxygenated species (butanol, methyl propyl ether and ethyl ethanoate). Rate constants were determined using on-the-fly canonical variational transition-state theory with small-curvature tunneling and multi-structural torsional anharmonicity. The calculated kinetics data were compared with previous reported results obtained from traditional transition state theory with unsymmetrical Eckart tunneling and the 1-D hindered rotor treatment. Additionally, this study investigated the effects of recrossing corrections and small-curvature tunneling, revealing the differences between different tunneling treatment and the influence of recrossing on reaction kinetics. These findings provide critical insights into reaction mechanisms and offer alternative kinetic data for advancing ammonia-hybrid combustion models. The work emphasizes the necessity of accounting for anharmonicity and multi-structural effects in rate constants and thermochemistry calculations, particularly for relative larger molecules with multiple conformers.

Keywords: Kinetics; Multi-structural effect; $\dot{N}H_2$ radical; H-atom abstraction; Tunneling effect

*Corresponding author.

1. Introduction

Nowadays, quantum chemistry methodologies offer several approaches for handling hindered internal rotations [1], each with distinct advantages in terms of accuracy and computational efficiency: (1) the single structure harmonic oscillator approximation, which considers only the most stable conformer while treating all vibration modes as harmonic oscillators; (2) the one-dimensional hindered rotor (1-D HR) treatment that specifically models low-frequency modes between heavy atoms as 1-D internal rotations; and (3) The multi-structural approximation with torsional anharmonicity (MS-T) [2,3], which explicitly accounts for multiple conformational structures generated by torsional motions. Among these, the latter two methods have gained particularly prominence in quantum chemistry studies due to their superior accuracy. The choice of methodology impacts the calculated kinetic and thermodynamic properties, making comparative studies of these different treatments an ongoing research focus in computational chemistry.

Ammonia (NH_3) has gained significant attention as a clean fuel alternative, addressing both fossil fuel depletion and stringent emission requirements [4,5]. While NH_3 exhibits lower reactivity than conventional fuels, blending it with more reactive compounds offers a practical approach for implementation in existing engines [6,7]. Alkanes are

View Article Online
DOI: 10.1039/D5CP04721H

Open Access Article. Published on 02 June 2026. Downloaded on 6/3/2026 5:39:24 AM.
This article is licensed under a Creative Commons Attribution 3.0 Unported Licence.

Physical Chemistry Chemical Physics Accepted Manuscript

promising candidates for blending with NH_3 to create hybrid fuels [8-10], effectively addressing the low reactivity and ignition challenges of NH_3, particularly at lower temperatures. Their high energy density, favourable ignition characteristics, and efficient combustion behaviour enhance combustion stability and improve overall engine performance [11,12]. Additionally, their compatibility with existing storage and transport infrastructure facilitates practical implementation. For instance, *n*-butane and *n*-pentane possess high volatility, ensuring efficient vaporization and enhancing cold-start performance in NH_3 blends. *iso*-Butane and *iso*-pentane, with their branched structure, offer higher octane numbers, reducing engine knock and improving combustion efficiency. *n*-Heptane, known for its low octane number, serves as a benchmark for ignition quality, enhancing the ignition characteristics of NH_3 blends in compression-ignition engines. *iso*-Octane, with its high-octane number, significantly reduces knock tendencies, ensuring stable and efficient combustion when combined with NH_3 in spark-ignition engines.

n-Butanol demonstrates superior characteristics among alcohol-based biofuels, serving both as an efficient fuel and performance-enhancing additive [13,14]. When derived from renewable feedstocks, it provides substantial environmental advantages by reducing fossil fuels dependence and lowering lifecycle carbon emissions. The fuel exhibits a high energy density (29.2 MJ/L) comparable to gasoline and approximately 25% higher than ethanol [15], enabling superior energy output in combustion application. Its advantageous physicochemical properties including reduced volatility, lower vapor pressure and corrosivity minimize volatile organic compounds (VOCs) emissions while maintaining excellent compatibility with existing fuel infrastructure components. The *n*-butanol/NH_3 blend system presents particular promise [16], as both fuels share liquid-phase storage compatibility, facilitating seamless integration into current distribution networks. Furthermore, high octane rating of *n*-butanol significant enhances the anti-knock performance of fuel blends, improving both combustion efficiency and engine operational stability.

Methyl propyl ether (MPE) [17,18] and Ethyl ethanoate (EE) [19] have emerged as versatile biofuel components, serving as representative benchmarks for ether and ester fuel families due to their physicochemical properties. MPE demonstrates particularly attractive characteristics for renewable fuel applications, including a high energy density and superior combustion performance. Its high cetane number ensures efficient ignition in compression-ignition engines, while the relatively low boiling point (39°C) promotes rapid vaporization — particularly advantageous for cold-start conditions. The oxygenated structure of MPE facilitates cleaner combustion, typically reducing particulate matter and carbon monoxide emissions compared to conventional diesel fuels [17]. Ethyl ethanoate (EE) exhibits excellent volatility and a high oxygen content, promoting more completed combustion with reduced emissions. Its compatibility with existing fuel systems and production pathways from renewable sources [20] further enhancing its sustainability credentials. The potential for blending either MPE or EE with NH_3 presents exciting opportunities to develop hybrid fuel systems that combine the combustion advantages of these oxygenates with the environmental benefits of ammonia, potentially creating next-generation renewable fuel formulations.

With optimized blending ratios and combustion conditions, these high-reactivity-ammonia mixtures could provide a high-performance, low-emission alternative fuel solution for transportation, power generation, and industrial sectors, supporting global efforts toward carbon neutrality. H-atom abstraction (HAA) from blended fuels by $\dot{N}H_2$ radicals is one of most important C–N cross reactions and plays a vital role in constructing ammonia-hybrid combustion mechanisms [21-23]. Recent theoretical studies have been carried out to systematically investigated H-atom abstraction from various hydrocarbon fuels, including alkanes [24], alcohols [25], ethers [25] and esters [26], by $\dot{N}H_2$ radicals. These theoretical calculation studies employed 1-D torsional treatment to account for the low-frequency torsional modes and used conventional transition state theory with Eckart tunnelling correction [27] to calculate rate constants across a temperature range of 500–2000 K. To improve the understanding and accuracy of reaction kinetics for larger fuel molecules and to validate two commonly used methods for rate constant calculations, this work is motivated by assessing the influence of multi-structural effects on rate constants and thermodynamic properties. Previous studies have often overlooked these effects, relying solely on the lowest-energy conformers of reactants and transition states, despite providing useful kinetic parameters for various HAA reaction types.

The primary objective of this study is to evaluate the impact of multi-structural effects on both kinetics and thermodynamics by comparing the 1-D hindered rotor treatment with a multi-structural method incorporating torsional anharmonicity. This comparison is carried out for HAA reactions by $\dot{N}H_2$ radicals from a representative set of alkanes and oxygenated biofuels taken the recrossing and small-curvature tunneling effects into consideration.

2. Theoretical and computational methods

2.1 Electronic structure calculations

To maintain consistency with prior computational studies employing 1-D hindered rotor treatments, the M06-2X [28] density functional combined with the 6-311++G(d,p) [29,30] basis set was adopted for distinguishable conformer searches and structural optimizations of the reactants and saddle points. For initial structure generation, the torsional angles of the reactants were sampled at five equal increments, corresponding to 72°, 144°, 216°, 288°,

View Article Online
DOI: 10.1039/D5CP04721H

Open Access Article. Published on 02 June 2026. Downloaded on 6/3/2026 5:39:24 AM.
This article is licensed under a Creative Commons Attribution 3.0 Unported Licence.

Physical Chemistry Chemical Physics Accepted Manuscript

and 360°, while those of transition states were divided into three increments (120°, 240° and 360°) to account for coupled internal torsional rotors. Distinguishable conformers were identified from optimized geometries based on root mean square deviation and energy deviation. Vibrational frequency calculations were performed at the M06-2X [28]/6-311++G(d,p) level of theory, with scaling factors of 0.970 and 0.983 applied to correct the zero-point energies (ZPE) and vibrational frequencies, respectively [31]. All reactants and products were confirmed to have no imaginary frequencies, and each saddle point has only one imaginary frequency.

Electronic structure calculations for all species used Gaussian 16 program [32]. SCF calculations were converged using the criteria of energy change (ΔE) < 10^{-8} a.u. and density change (ΔD) < 10^{-10} a.u. in Gaussian16. Geometry optimizations employed the Opt=Tight keyword. The convergence thresholds were: maximum force < 0.00045 a.u., RMS force < 0.0003 a.u., maximum displacement < 0.0018 a.u., RMS displacement < 0.0012 a.u. The Int=grid=99974 was used for all DFT calculations.

2.2 Multi-structure and torsional anharmonicity

The multi-structural local harmonic (MS-LH) [33] and multi-structural torsional anharmonicity (MS-T) [2,3] methods were employed to calculate partition functions and thermodynamic properties. The MS-T method accounts for all distinguishable conformers arising from multiple minima due to torsional degrees of freedom. It enhances the accuracy of harmonic approximations by incorporating torsional anharmonicity and coupling of torsions with overall rotation with each another. The conformational-rovibrational partition function in MS-T method is expressed as:

$$Q_{\text{con-rovib}}^{\text{MS-T(G)}} = \sum_{j=1}^{J} Q_{\text{rot},j} \exp(-\beta U_j)\, Q_j^{\text{HO}} \prod_{\eta=1}^{t} f_{j,\eta} \tag{1}$$

Where J is the number of distinguishable structures, U_j is the energy of structure j, $Q_{\text{rot},j}$ is the rotational partition function for structure j, Q_j^{HO} is the harmonic oscillator vibrational partition function for structure j, t is the number of torsions, and $f_{j,\eta}$ is an internal-coordinate torsional anharmonicity factor. If $f_{j,\eta}$ is set to unity, this partition function reduces to the MS-LH partition function.

The correction factor for multi-structural torsional anharmonicity is defined as:

$$F^{\text{MS-T}}(T) = \frac{Q_{\text{con-rovib}}^{\text{MS-T}}(T)}{Q_{\text{con-rovib}}^{\text{SS-HO}}(T)} \tag{2}$$

where $Q_{\text{con-rovib}}^{\text{SS-HO}}$ is the single structure harmonic oscillator partition function. Similarly, the multi-structural correction factor that accounts for vibrational anharmonicity while neglecting torsional anharmonicity is defined as:

$$F^{\text{MS-LH}}(T) = \frac{Q_{\text{con-rovib}}^{\text{MS-LH}}(T)}{Q_{\text{con-rovib}}^{\text{SS-HO}}(T)} \tag{3}$$

Multi-structural calculations were performed in the MSTor 2023 program [34], detailed description is available in MSTor manual [34].

2. 3 Thermochemistry calculations

The 1-D hindered rotor treatment result together with the optimized geometries, vibrational frequency calculations was employed in the partition function calculations, which were subsequently used to calculate thermochemical properties for the selected representative species at different temperatures. The atomization method, combined with the composite calculations was employed at the CBS-QB3 [35], CBS-APNO [36], G3 [37] and G4 [38] levels of theories to calculate the enthalpies of formation at 0 K for stable molecules involved in the reactions. Based on these inputs, the partition functions and thermodynamic properties, including the standard enthalpy of formation ($\Delta H_{\text{f,298K}}$), entropy at 298 K ($S_{298\text{K}}$), and heat capacity C_{p} were calculated using the ThermP code [39]. The calculated thermochemistry data were subsequently fitted to NASA polynomial format using the PAC99 code [39-41].

The MS-T calculates partition functions and thermodynamic functions of species differently. Based on the enthalpy values calculated using the MS-T method, the standard enthalpies of formation adopted by He et al. [42] were employed. A hypothetical formation reaction, x C(g) + y/2 H_2(g) + z/2 O_2(g) = $C_xH_yO_z$(g), was constructed to calculate the gas phase standard enthalpy of formation for $C_xH_yO_z$ species:

$$\begin{aligned}\Delta H_{\text{f,298K}}(C_xH_yO_z) = {} & H_{\text{f,298K}}(C_xH_yO_z) - x\, H_{\text{f,298K}}(C) - y/2\, H_{\text{f,298K}}(H_2) - z/2\, H_{\text{f,298K}}(O_2) \\ & + x\, \Delta H_{\text{f,298K}}(C) + y/2\, \Delta H_{\text{f,298K}}(H_2) + z/2\, \Delta H_{\text{f,298K}}(O_2)\end{aligned} \tag{4}$$

2.4 Rate constants calculations

Rate constants were calculated over the temperature range of 298.15–2000 K using the multi-structural canonical variational theory combined with the small-curvature tunneling (MS-CVT/SCT):

$$k^{\text{MS-CVT/SCT}}(T) = \alpha^{\text{MS-T}}(T) \kappa^{\text{SCT}} I^{\text{CVT}}(T) k^{\text{TST}}(T) \tag{5}$$

View Article Online
DOI: 10.1039/D5CP04721H

Open Access Article. Published on 02 June 2026. Downloaded on 6/3/2026 5:39:24 AM.
This article is licensed under a Creative Commons Attribution 3.0 Unported Licence.

Where $k^{TST}(T)$ is the rate constant calculated using the canonical transition state theory (C-TST) method implemented in the POLYRATE software. $\alpha^{MS-T}(T)$ is the multi-structural torsional anharmonicity factor on reaction kinetics:

$$\alpha^{MS\text{-}T}(T)=\frac{F_{TS}^{MS\text{-}T}(T)}{F_{reactant1}^{MS\text{-}T}(T)F_{reactant2}^{MS\text{-}T}(T)} \quad (6)$$

κ^{SCT} is the small-curvature tunneling probability [43], and $k^{CVT}(T)$ is the rate constant calculated using canonical variational transition-state theory (CVTST) [44], incorporating recrossing corrections. Conventional transition-state theory (TST) typically considers a single saddle point as the sole transition state separating reactants and products. In contrast, CVTST accounts for a sequence of TSs along the minimum energy path (MEP), the distance along the MEP is called *s*. The rate constants are determined by minimizing the free energy barrier along the forward reaction pathway at a given temperature. This can be expressed as the product of the canonical recrossing transmission coefficient, $\Gamma^{CVT}(T)$, and the conventional transition state theory rate constant, offering a more accurate representation of the reaction kinetics:

$$k^{CVT}(T)=\min_{s} k^{TST}(T,s)=\Gamma^{CVT}(T)k^{TST}(T) \quad (7)$$

The Polyrate 17-C [45] and Gaussrate 17-B [45,46] programs are uesed to compute $k^{CVT}(T)$, κ^{SCT}, and vibrationally adiabatic ground-state energies $V_a^G(s)$, where:

$$V_a^G(s)=V_{MEP}(s)+\varepsilon^G(s) \quad (8)$$

Where $\varepsilon^G(s)$ is the ZPE of structure at a selected location along the MEP.

For single-structure rate constants, the most stable conformer of the reactant and TS is adopted. The Page–McIver method and the reorientation of the dividing surface algorithm [47] are employed to compute the MEPs along curvilinear internal coordinates. The reaction coordinate s for MEP calculation ranges from –1.0 Å to 1.0 Å, with a step size of 0.005 Å and a mass scaled of 1 amu. Hessians are updated every nine steps.

3. Results and discussion

3.1 Fuel molecules selected

To systematically investigate the impact of hindered rotor treatments on kinetic and thermodynamic predictions, seven C4–C8 alkanes and three oxygenated fuel molecules with multiple conformers were selected. Fig. 1 presents the molecular structures, compound names and the labeling scheme for various HAA sites, which follows the convention established in our previous studies [24-26]. Conformational analysis indicated that straight-chain alkanes generally exhibit greater conformational diversity than their branched isomers with the same carbon number. For example, *n*-pentane possesses seven distinguishable conformers, whereas *iso*-pentane has three and neopentane only one. This trend aligned with chemical intuition and supported by prior theoretical studies by Truhlar et al. [48] and Gao et al. [49], served as the basis for selecting straight-chain oxygenated species for multi-structural analysis. The oxygenated compounds of butanol, methyl propyl ether and ethyl ethanoate were chosen to represent the chemical families respectively and maintain the molecule chain lengths for conformational analysis. Due to the significant computational demands of MS-T calculations for larger molecules like *n*-heptane and *iso*-octane, only their dominant channels were examined in this study.

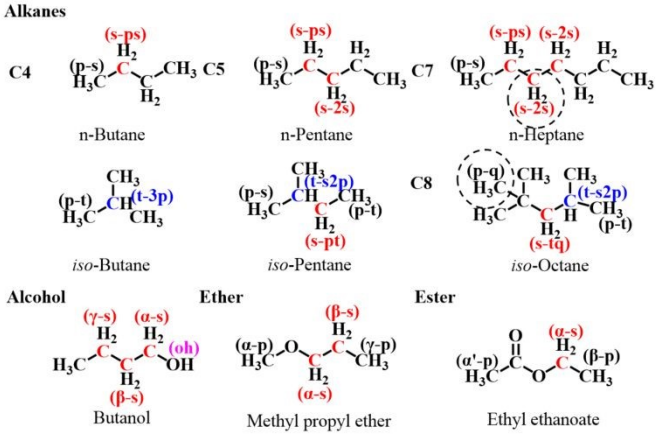

Fig. 1. Molecular structures of target species and the abstracted hydrogen atom sites investigated in this study (black: primary carbon, red: secondry carbon, blue: tertiary carbon, pink: hydroxyl).

3.2 Thermodynamics

Physical Chemistry Chemical Physics Accepted Manuscript

View Article Online
DOI: 10.1039/D5CP04721H

Open Access Article. Published on 02 June 2026. Downloaded on 6/3/2026 5:39:24 AM.
This article is licensed under a Creative Commons Attribution 3.0 Unported Licence.

Physical Chemistry Chemical Physics Accepted Manuscript

The standard enthalpy of formation ($\Delta H_{f,298K}$) and entropy at 298 K (S_{298K}), calculated using both 1-D torsional treatment and MS-T method, were compared with literature results including the Active Thermochemical Tables (ATcT) [22], the Third Millennium Ideal Gas and Condensed Phase Thermochemical Database for Combustion (referred as Burcat's database in this work) [50], and the NIST Chemistry Webbook [51,52]. The comparison results are shown in supplementary information (SI) Table S1.

To reduce the potential uncertainty from the different databases, Fig. 2 (a) presents the absolute deviation between calculated standard enthalpy of formation and ATcT refence values, while Fig. 2 (b) shows the corresponding deviations for entropies at 298 K relative Burcat's database. Enthalpy of formation calculated by both of the two computational methods are within 1.00 kcal mol^{-1} difference from each other except for *iso*-octane, where the 1-D torsional treatment shows a deviation of 1.33 kcal mol^{-1} from the literature [22]. Mean unsigned error (MUE) is 0.58 kcal mol^{-1} for $\Delta H_{f,298K}$ and 1.01 cal mol^{-1} K^{-1} for S_{298K} by using the 1-D torsional treatment method, that are 0.24 kcal mol^{-1} and 0.28 cal mol^{-1} K^{-1}, respectively by using the MS-T approach. These results show that the MS-T method is relatively more accurate in calculating the thermochemistry data. The calculated heat capacities across species showed systematic increases with molecular size, exhibiting good agreement between the two partition function treatments (within 0.48 cal mol^{-1}K^{-1}) as well as with database benchmarks. Detailed comparison between this work and the ones from the literature is shown in SI Table S2.

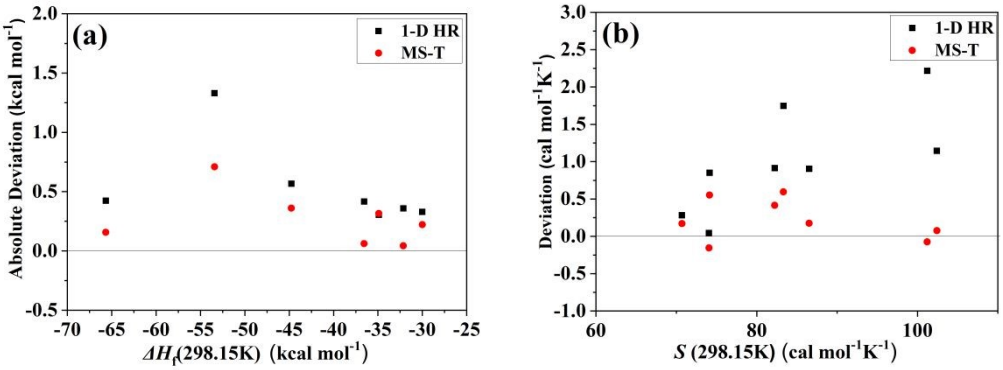

Fig. 2. Deviation between calculated (a) standard enthalpy of formation (b) entropy at 298 K and the corresponding literature data for selected species in Fig. 1.

3. 3 Multi-structural torsional anharmonicity

A systematic conformer search for HAA reactions with $\dot{N}H_2$ radicals revealed distinct conformational landscapes across different molecular systems. Multiple conformational structures are generated by internal rotations. Different conformations forming from the torsion of the C–H–NH_2 moiety were included. Nitrogen inversion was not considered. For the *n*-butane, 3 reactant conformers were identified, with 20 and 10 transition state conformers located at the p-s and s-ps sites, respectively. *iso*-Butane exhibited 1 reactant conformer while 10 and 2 transition state conformers located at the p-t and t-3p sites. For *n*-pentane, 7 reactant conformers were found, alongside 33, 24, and 18 transition state conformers at the p-s, s-ps, and s-2s sites, respectively. *iso*-Pentane displayed 3 reactant conformers and 20, 32, 12, and 12 transition state conformers located at the p-s, t-s2p, s-pt, and p-t sites, respectively. Larger alkanes showed increased conformational complexity. *n*-Heptane yielded 58 reactant conformers and 67 transition state conformers at s-ps site, while *iso*-octane produced 6 reactant conformers and 62 transition state conformers found at p-q site. Oxygenated species exhibited particularly rich conformational diversity. Butanol featured 27 reactant conformers and 54, 42, 100, and 86 transition state conformers located at OH, α-s, β-s and γ-s sites. For the methyl propyl ether, 9 reactant conformers were included, alongside 45, 24, 24, and 50 transition state conformers at the α-p, α-s, β-s, and γ-p sites, respectively. Ethyl ethanoate presented 7 reactant conformers and 34, 18, and 36 transition state conformers located at α'-p, α-s and β-s/γ-p sites. All conformer counts include enantiomeric pairs, as determined by rigorous symmetry analysis. These results highlight the substantial variations in conformational complexity as a function of molecular size, functional group, and abstraction site type.

The effect of multi-structural torsional anharmonicity on rate constants is represented by the factor $\alpha^{MS\text{-}T}(T)$, which is defined as the ratio of $F_{TS}^{MS\text{-}T}(T)$ to $F_{reactant}^{MS\text{-}T}(T)$. In this study, since one of the reactants is the $\dot{N}H_2$ radical, which does not exhibit multi-structural with torsional anharmonicity effects, only the effects of TSs and the other reactant need to be considered. The individual contributions of multi-structural effects and torsional anharmonicity to the reaction kinetics can be evaluate by the ratio $\alpha^{MS\text{-}T}(T)/\alpha^{MS\text{-}LH}(T)$, which quantifies the impact of torsional anharmonicity on rate constants.

View Article Online
DOI: 10.1039/D5CP04721H

Open Access Article. Published on 02 June 2026. Downloaded on 6/3/2026 5:39:24 AM.
This article is licensed under a Creative Commons Attribution 3.0 Unported Licence.

Fig. 3 present the influence of torsional anharmonicity, namely $\alpha^{\text{MS-T}}(T)/\alpha^{\text{MS-LH}}(T)$, on reaction rate constant across different HAA sites. The rotation of the methyl group in conformers does not lead to distinguishable structures, so it does not contribute to multi-structure effects. However, the torsions involving the methyl group couple with other torsions, thereby contributing to the torsional anharmonicity effects. As shown in Fig. 3, the value of $\alpha^{\text{MS-T}}(T)/\alpha^{\text{MS-LH}}(T)$ for primary carbon sites range from 0.15 to 0.65, for secondary carbon sites from 0.23 to 0.76, for tertiary carbon sites from 0.19 to 0.46, and for the hydroxyl site from 0.44 to 0.61. Regardless of the specific site characteristics, the overall impact of torsional anharmonicity consistently below 0.8, which decreases the rate constants systematically. This result reveals that considering only the anharmonicity arising from conformational distributions while neglecting coupled torsional potentials leads to the rate constants being overestimated by approximately 20–85%. These findings highlight the critical importance of incorporating complete torsional coupling effects in kinetic predictions, particularly for systems exhibiting complex multi-dimensional potential energy surfaces. The observed universal suppression effect across all site types suggests torsional anharmonicity represents a fundamental correction factor that should be routinely included in HAA kinetic calculations.

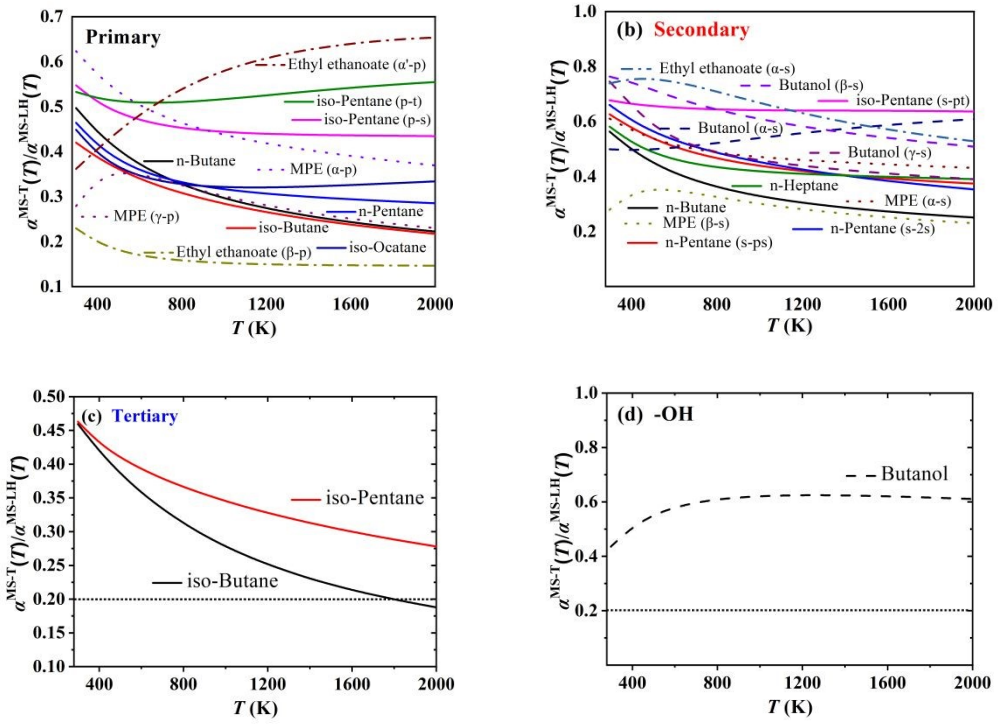

Fig. 3. Effects of torsional anharmonicity on reaction rate constants as a function of temperature for various reactants and different types of HAA.

The $\alpha^{\text{MS-T}}(T)$ values for different types of HAA reaction sites, including primary carbon, secondary carbon, tertiary carbon, and hydroxyl group, are shown in Fig. 4. The multi-structural torsional anharmonicity factor ($\alpha^{\text{MS-T}}(T)$) exhibits a temperature-dependent influence on reaction rate constants, with values larger than one, leading to rate constant enhancement and vice versa. The factor values for the same type of site across different species exhibit significant variation. For example, the $\alpha^{\text{MS-T}}(T)$ values for the primary HAA site of *iso*-octane range from 9.3 to 10.6, whereas those for *iso*-pentane vary from 2.5 to 5.0. Substantial differences also exist in the factor values for similar sites within the same species. For methyl propyl ether, the value for the α-p site ranges from 7.0 to 7.7, whereas that for the γ-p site ranges from 0.2 to 1.5. For the secondary carbon sites in butanol, the values for the β-s and γ-s sites exhibit strong temperature dependence, ranging from 0.3 to 6.7. In contrast, the value for the α-s site remains below 0.7 across the whole temperature range. A comprehensive analysis reveals that the temperature dependence of $\alpha^{\text{MS-T}}(T)$ cannot be reliably inferred from reaction site type alone, as different HAA types exhibit no consistent trends in torsional anharmonicity behavior. This lack of class-specific patterns underscores the necessity of first-principles calculations for each distinct reaction pathway, requiring rigorous

Physical Chemistry Chemical Physics Accepted Manuscript

View Article Online
DOI: 10.1039/D5CP04721H

Open Access Article. Published on 02 June 2026. Downloaded on 6/3/2026 5:39:24 AM.
This article is licensed under a Creative Commons Attribution 3.0 Unported Licence.

Physical Chemistry Chemical Physics Accepted Manuscript

evaluation of the full conformational distributions of both reactants and transition states, as well as the internal torsional modes and associated energy landscapes of flexible molecular frameworks. This detailed analysis can derive the rovibrational partition functions accurately and ultimately obtain accurate $\alpha^{\text{MS-T}}(T)$ values that properly account for the complex interplay of multi-structural effects in kinetic predictions.

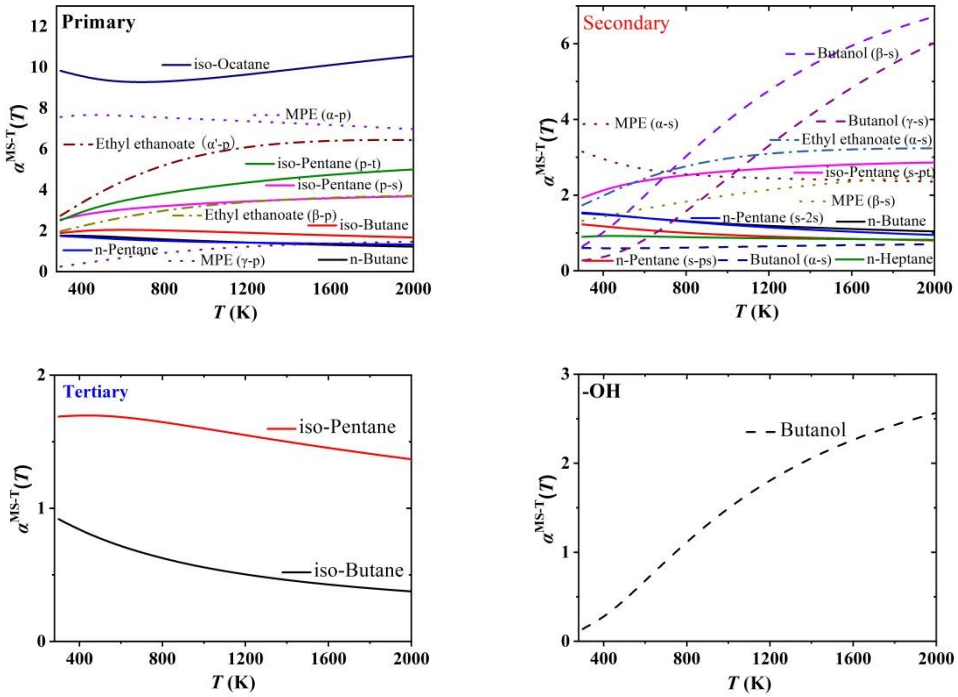

Fig. 4. Multi-structural torsional anharmonicity factors as a function of temperature for reactions at different H-abstraction type of various reactants.

3.4 Recrossing and tunneling effects

Canonical variational transition state theory (CVTST) calculations provided quantitative insight into recrossing effects during HAA by $\dot{N}H_2$ radicals, as evidenced by the transmission coefficients Γ^{CVT} shown in Fig. 5 for different reaction channels. Alkane reactant systems exhibit consistent site dependent recrossing behavior with transmission coefficients Γ^{CVT} of 0.70–0.95 for primary, 0.82–0.98 for secondary, and 0.90–1.00 for tertiary sites. Oxygenated fuels demonstrate more complicated dynamics and the displacement of the generalized transition state along the reaction coordinate serves as the primary indicator of variational strength, for example of butanol where the α-site abstraction displays significantly stronger variational effects (generalized transition state displacement progressing from –0.03 Bohr at 298 K to –0.067 Bohr at 2000 K) compared to the β-site (–0.015 to –0.023 Bohr). Furthermore, branched alkanes consistently show coefficients nearer to unity than their linear counterparts, indicating substantially reduced recrossing effects. The predominance of sub-unity coefficients (typically 0.7–0.95) provides compelling evidence that conventional transition state theory systematically overestimates reaction rates by 5–30%, with the degree of overestimation being highly dependent on both molecular structure and specific abstraction site characteristics.

View Article Online
DOI: 10.1039/D5CP04721H

Open Access Article. Published on 02 June 2026. Downloaded on 6/3/2026 5:39:24 AM.
This article is licensed under a Creative Commons Attribution 3.0 Unported Licence.

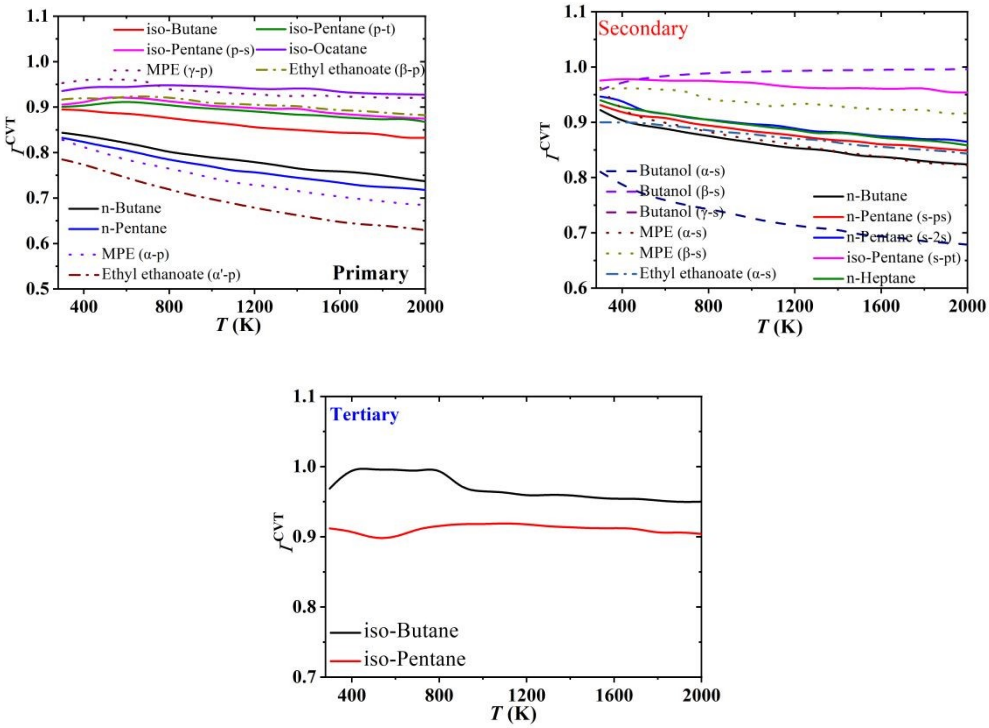

Fig. 5. Canonical recrossing transmission coefficients for each studied reaction at various temperatures

To investigate the influence of quantum tunneling effects on reaction rate constants, the temperature-dependent tunneling transmission coefficients κ calculated using the small-curvature tunneling (SCT) method are presented in Fig. 6, with Eckart tunneling (ET) corrections included for comparison. The SCT transmission coefficients account for both quantum mechanical tunneling and non-classical reflection above the effective barrier. Tunneling effects can be rationalized based on the shape of the vibrationally adiabatic ground-state potential energy curve—the narrower and higher barriers typically exhibit stronger tunneling contributions, as the tunneling probability increases with barrier steepness. HAA at primary sites generally involves larger reaction barriers, leading to more significant tunneling effects compared to secondary or tertiary sites. To confirm that the reaction coordinate range for MEP calculation of –1 to 1 Å is sufficient to describe the low-temperature tunneling effect, the channels at the β-p site of ethyl ethanoate (EE) and the p-s site of n-butane were selected for validation with different reaction coordinate ranges, and the results are presented in Fig. S2 of the SI. In summary, expanding the reaction coordinate range for MEP calculation has no contribution to κ at temperature range from 298.15 K to 2000 K. Therefore, it is reasonable to adopt the range of –1 to 1 Å in this work.

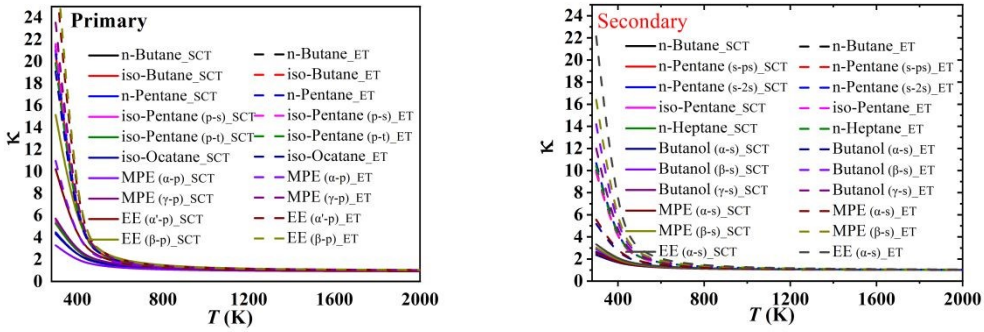

Physical Chemistry Chemical Physics Accepted Manuscript

View Article Online
DOI: 10.1039/D5CP04721H

Open Access Article. Published on 02 June 2026. Downloaded on 6/3/2026 5:39:24 AM.
This article is licensed under a Creative Commons Attribution 3.0 Unported Licence.

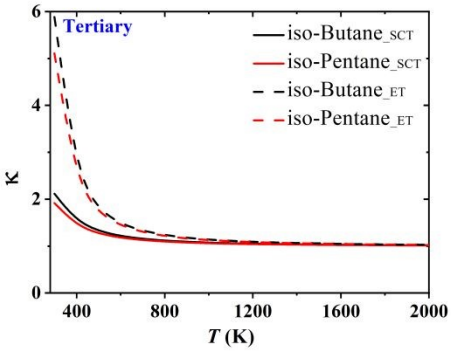

Fig. 6. Multi-dimensional SCT and one-dimensional ET tunneling transmission coefficients as a function of temperature for each studied reaction.

3.5 Kinetics

Table 1
Electronic barriers (kcal mol^{-1}) comparison among different HAA reaction channels.

	Species	Primary	Secondary	Tertiary	-OH
C4	***n*-Butane**	9.55[1](p-s) 8.41[2] 8.25[3]	7.31[1](s-ps) 6.24[2] 6.00[3]	–	
	***iso*-Butane**	9.50[1](p-t) 8.21[2] 11.40[4]	–	5.94[1](t-3p) 5.08[2] 7.30[4]	
C5	***n*-Pentane**	9.43[1](p-s) 8.35[2]	7.21[1](s-ps) 6.20[2] 7.34[1](s-2s) 6.07[2]	–	
	***iso*-Pentane**	9.51[1](p-s) 8.34[2] 9.33[1](p-t) 8.04[2]	7.26[1](s-pt) 6.01[2]	5.65[1](t-s2p) 4.58[2] 4.35[3]	
	Neopentane	9.32[1](p-q) 8.13[2]	–	–	
C7	***n*-Heptane**	–	7.07[1](s-ps) 6.11[2]	–	
C8	***iso*-Octane**	8.94[1](p-q) 7.84[2]	–	–	
Alcohol	**Butanol**	–	5.35[1](α-s) 4.15[2](α-s) 7.10[1](β-s) 5.59[2](β-s) 7.59[1](γ-s) 6.31[2](γ-s)		7.58[1] 4.98[2]
Ether	**Methyl propyl ether**	7.09[1](α-p) 6.19[2](α-p) 9.69[1](γ-p) 8.47[2](γ-p)	5.45[1](α-s) 4.42[2](α-s) 7.40[1](β-s) 6.00[2](β-s)		
Ester	**Ethyl ethanoate**	9.20[1](α'-p) 8.26[2](α'-p) 10.30[1](β-p) 9.04[2](β-p)	6.83[1](α-s) 5.76[2](α-s)		

[1] Previous QCISD(T)/CBS calculations (this work series).
[2] This work at M06-2X/6-311++G(d,p) level.
[3] Siddique et al. at CBS-QB3 level [73].

Physical Chemistry Chemical Physics Accepted Manuscript

View Article Online
DOI: 10.1039/D5CP04721H

[4] Mebel et al. at G2M level [74].

As shown in Table 1, the electronic barriers calculated at the M06-2X/6-311++G(d,p) level are systematically lower by approximately 1 kcal mol–1 compared to the benchmark values obtained at the QCISD(T)/CBS//M06-2X/6-311++G(d,p) level of theory, which would introduce an error of ~20% in TST calculated rate constants over the temperature range of 500–2000 K.

Anomalous transverse imaginary frequencies occurred during sampling along the minimum energy path (MEP). The effects of these transverse imaginary frequencies on vibrationally adiabatic potentials, free energy profiles and rate constants $k^{\text{MS-CVT/SCT}}(T)$ were comprehensively discussed. Fig. S3 in the supporting information compares the results with and without interpolation correction modes of abnormal imaginary frequencies. Transverse imaginary frequencies cause free energy profile truncation and significant free energy reduction, which is more severe at high temperatures. The impact on the rate constants also increases with rising temperature. Channel-dependent effects arise from differences in the number and spatial range of these imaginary frequencies. For instance, MEP for the H-atom abstraction at the *n*-butane p-s site has two transverse imaginary frequencies near the saddle point, whereas the ethyl ethanoate β-p site only has two between –0.3 and –1.2 Å and one elsewhere. Given that all channels have 1-2 uncorrected transverse imaginary frequencies near the saddle point, we estimate a 35% uncertainty in $k^{\text{MS-CVT/SCT}}(T)$ arising from this issue.

Analysis of the comparison results reveals that the presence of transverse imaginary frequencies causes truncation of the free energy profile and a significant decrease in the free energy at the corresponding coordinate points, and this effect is more pronounced at high temperatures. The impact on the rate constants also increases with rising temperature. Furthermore, the rate constants of different reaction channels are affected to different extents, which is attributed to variations in the number and existence range of transverse imaginary frequencies.

The rate constants for the HAA reactions by $\dot{N}H_2$ radicals calculated using the multi-structural canonical variational transition state theory with small-curvature tunneling and recrossing corrections ($k^{\text{MS-T\&CVT/SCT}}(T)$) over the temperature range of 298.15–2000 K are presented in Fig. 7 and Fig. 8. These results are compared with previous calculations employing the 1-D hindered rotor (1-D HR) treatment in MESS [74] combined with conventional transition state theory and Eckart tunneling corrections ($k^{\text{TST/ET}}(T)$) over the temperature range of 500–2000 K. The comparative analysis reveals generally good agreement between the two methods across all reaction channels. For the $\dot{N}H_2$ + alkane systems, the largest discrepancy (a factor of 2.27 at 500 K) was observed for the primary site abstraction in *iso*-octane over 500–2000 K and the rate constants for other alkane reaction pathways showed excellent agreement with differences typically below 30%. In the low-temperature region (< 500 K), the rate constants from MS-T method were 15–20% lower than the 1-D HR method systematically, primarily due to more rigorous treatment of multi-conformational distributions and coupled torsional potentials. The comparison of rate constants obtained using the conventional TST with Eckart tunneling (TST/ET) and the multi-structural variational transition state theory with small-curvature tunneling and torsional anharmonicity (MS-T&CVT/SCT) reveals systematic differences across molecular classes. While the discrepancies between the two methods remain within a factor of ~2 across the entire temperature range for most alkanes—highlighting relativelymodest multi-structural and anharmonicity effects—significantly larger differences are observed for oxygenated species. For instance, at 500 K, the α-site hydrogen abstraction from ethyl acetate shows an MS-T&CVT/SCT rate constant that is over 2.5 times greater than its TST/ET counterpart. This pronounced deviation is attributed to the increased conformational flexibility introduced by functional groups such as –OH, –O–, and –COO–, which lead to a broader distribution of accessible conformers and more complex torsional energy landscapes. Consequently, the multi-structural effects and torsional anharmonicity corrections become critical in accurately capturing the kinetics of oxygenated fuel molecules—far more so than for structurally simpler hydrocarbons.

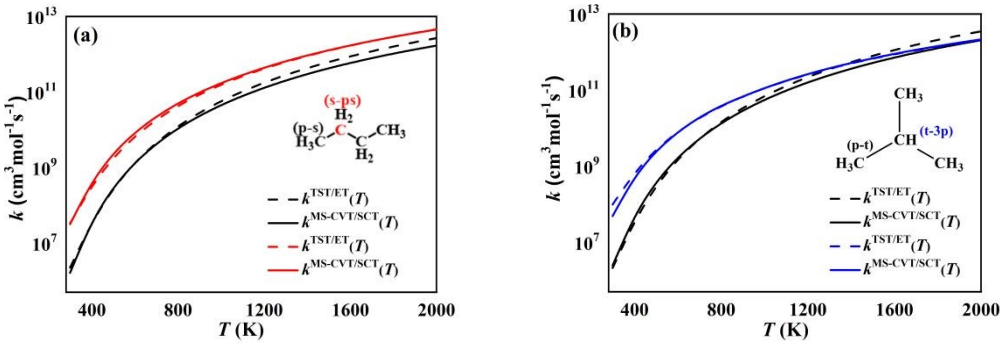

Open Access Article. Published on 02 June 2026. Downloaded on 6/3/2026 5:39:24 AM.
This article is licensed under a Creative Commons Attribution 3.0 Unported Licence.
Physical Chemistry Chemical Physics Accepted Manuscript

View Article Online
DOI: 10.1039/D5CP04721H

Open Access Article. Published on 02 June 2026. Downloaded on 6/3/2026 5:39:24 AM.
This article is licensed under a Creative Commons Attribution 3.0 Unported Licence.

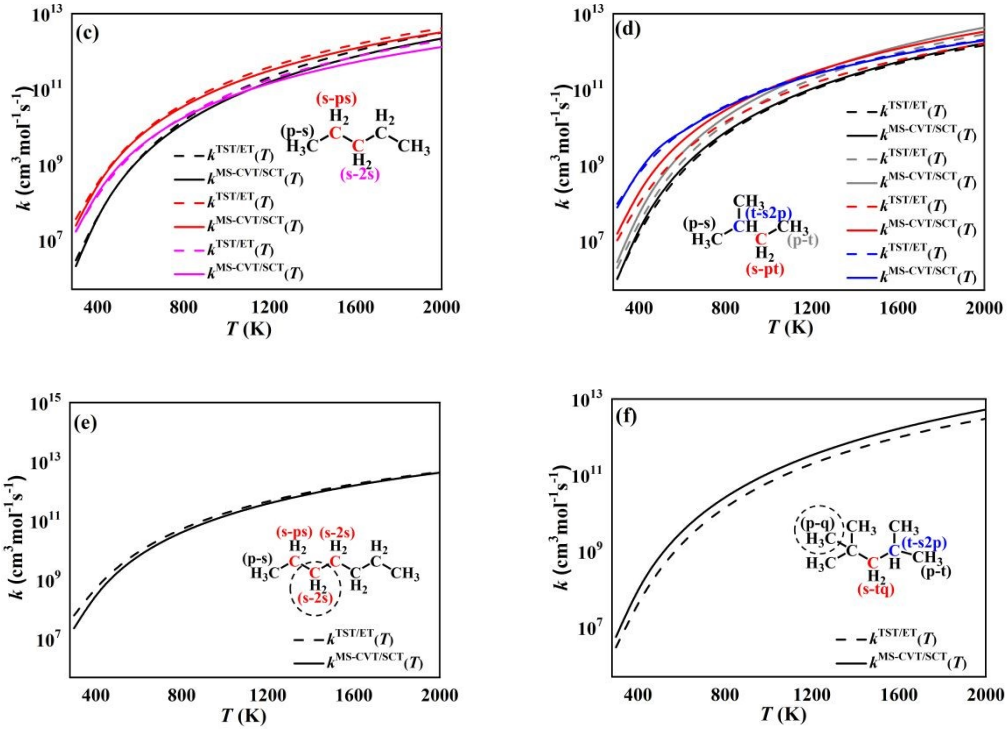

Fig. 7. Comparisons of rate constants (in $cm^3\ mol^{-1}\ s^{-1}$) for the H-atom abstraction reactions of various alkanes with the $\dot{N}H_2$ radical.

Fig. 8 presents a comparative evaluation of rate constants for $\dot{N}H_2$-mediated HAA from butanol, methyl propyl ether, and ethyl acetate, revealing systematic differences between the $k^{MS\text{-}T\&CVT/SCT}$ and $k^{TST/ET}$ methodologies. The most pronounced discrepancy occurs at ethyl acetate's α-s site, where the multi-structural approach yields rate constants 2.53, 2.31, and 1.87 times larger than the conventional treatment at 500 K, 1000 K, and 2000 K respectively. This variation stems principally from differential torsional treatments ($\alpha^{MS\text{-}T}/\alpha^{1\text{-}D\ HR}$ ratios of 1.69, 1.68, and 1.66 at corresponding temperatures), with secondary contributions arising from tunneling methodology variations (SCT vs. ET) and electronic barrier differences. Notably, although both the 1D HR-based TST with Eckart tunneling (TST/ET) and the multi-structural variational transition state theory with small-curvature tunneling (MS-T&CVT/SCT) yield rate constants within the commonly accepted two-fold uncertainty margin in computational kinetics, the MS-T&CVT/SCT approach requires significantly greater computational resources. In addition to harmonic frequency calculations, the MS-T framework necessitates extensive conformational sampling for both reactants and transition states, accurate hindered rotor scans for all flexible torsional modes, and high-resolution minimum energy path (MEP) calculations to capture variational effects and tunneling contributions. In contrast, the 1D-HR method relies on a single optimized geometry and a limited number of torsional scans, making it substantially more efficient. For the same reaction system, the MS-T&CVT/SCT method can require up to 5–10 times more CPU time and disk storage, depending on molecular complexity and the number of torsional degrees of freedom. Despite this computational cost, the accuracy gains are modest for saturated hydrocarbons, whereas for highly flexible or oxygenated species, the improvements become more pronounced and potentially necessary. The observed temperature-dependent convergence of results suggests diminishing methodological sensitivity at higher temperatures, particularly above 1000 K where quantum effects become less dominant.

Physical Chemistry Chemical Physics Accepted Manuscript

View Article Online
DOI: 10.1039/D5CP04721H

Open Access Article. Published on 02 June 2026. Downloaded on 6/3/2026 5:39:24 AM.
This article is licensed under a Creative Commons Attribution 3.0 Unported Licence.

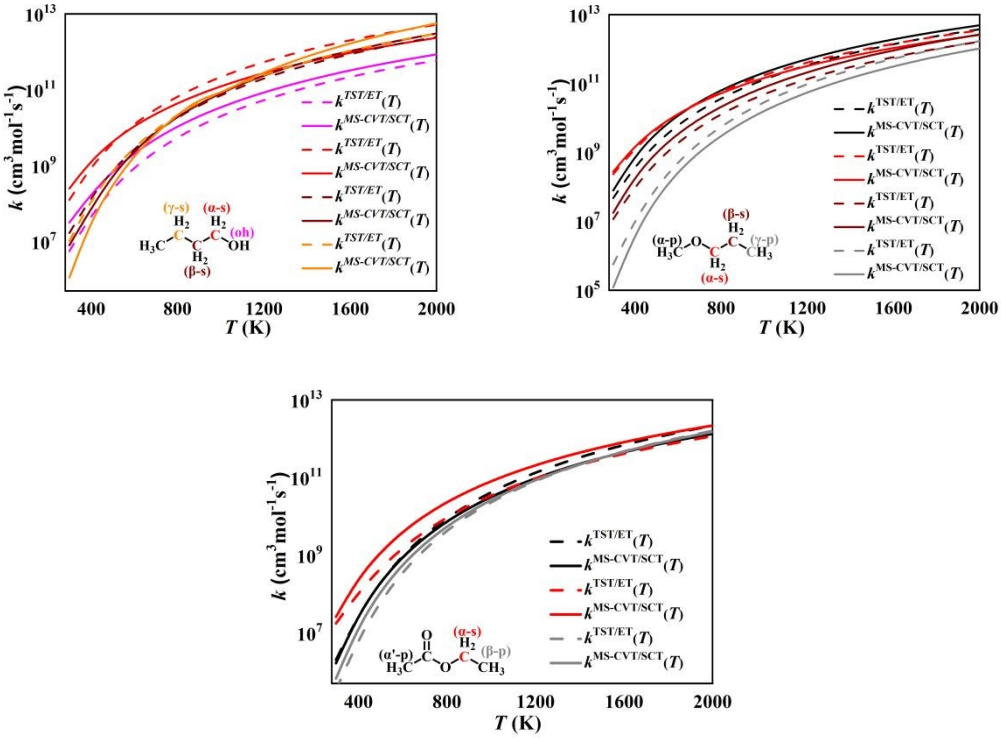

Fig. 8. Comparisons of rate constants (in $cm^3\ mol^{-1}\ s^{-1}$) for the H-atom abstraction reactions of butanol, methyl propyl ether and ethyl ethanoate with the $\dot{N}H_2$ radical.

4. Conclusions

In this work, multi-structural canonical variational transition state theory with small curvature tunneling was applied to calculate high-pressure limit rate constants for H-atom abstraction by $\dot{N}H_2$ radical from a series of representative alkanes, butanol, methyl propyl ether and ethyl ethanoate.

Two methods for treating hindered rotations, the 1-D hindered rotor treatment and the multi-structural treatment with torsional anharmonicity, were used to calculate the standard enthalpy of formation, entropy and heat capacity for nine representative compounds. The calculated values were compared with corresponding value in databases. Both hindered rotation treatments predicted thermochemical properties within a reasonable range, with the MS-T method generally showing closer agreement with the database benchmarks, as reflected in the lower mean unsigned errors (MUE is 0.24 kcal mol^{-1} and 0.28 cal mol^{-1} K^{-1} for MS-T, versus 0.58 kcal mol^{-1} and 1.01 cal mol^{-1} K^{-1} for the 1-D torsional treatment).

To investigate the effects of multi-structure and torsional anharmonicity on rate constants, the $\alpha^{MS\text{-}T}$, $\alpha^{MS\text{-}LH}$ and $\alpha^{MS\text{-}T}/\alpha^{MS\text{-}LH}$ factors on rate constants were calculated as a function of temperature. The results indicate that, the overall impact of torsional anharmonicity remains consistently within the range of 0.15–0.8 across all reaction site types, demonstrating a universal suppression effect on reaction rates. The temperature dependence of multi-structural torsional anharmonicity factors shows no predictable pattern based on reaction class, necessitating first-principles calculations for each individual reaction pathway. These calculations must explicitly account for complete conformational distributions of reactants and transition states, internal torsional modes of flexible molecular frameworks, and corresponding energy landscapes to derive accurate rovibrational partition functions and determine the resultant multi-structural torsional anharmonicity factors. Notably, these factors exhibit close agreement (generally within a factor of two) with correction factors obtained from 1-D HR treatments, validating the consistency between methodologies while highlighting the importance of pathway-specific analyses for precise kinetic predictions.

To illustrate the contribution of variational and tunneling effects to the site-specific kinetic data, recrossing and tunneling transmission coefficients were calculated. Recrossing corrections (transmission coefficients typically 0.7–0.95) systematically reduce rate constants, while tunneling effects are most significant at low temperatures (298.15–500 K), particularly for primary sites. The small-curvature tunneling (SCT) and Eckart methods show good agreement above 500 K (coefficients < 2.76) with maximum discrepancies of 1.2–1.8, though the MS-

Physical Chemistry Chemical Physics Accepted Manuscript

View Article Online
DOI: 10.1039/D5CP04721H

Open Access Article. Published on 02 June 2026. Downloaded on 6/3/2026 5:39:24 AM.
This article is licensed under a Creative Commons Attribution 3.0 Unported Licence.

Physical Chemistry Chemical Physics Accepted Manuscript

T&CVT/SCT approach yields different rates compared to 1-D HR-TST/ET method - notably *iso*-octane (2.27× at 500 K) and ethyl acetate α-sites (2.53× at 500 K) - due to improved treatment of multi-conformer systems, albeit at 5–10× greater computational cost. These results demonstrate that while the predictions of conventional TST/ET and MS-T&CVT/SCT methods are comparable at high temperatures (> 1000 K), they exhibit significant discrepancies for the low-temperature kinetics of oxygenated compounds and sterically hindered sites.

Author contributions

- **Jingwu Sun**: Investigation; Formal analysis; Data Curation; Writing - Original Draft
- **Zhaolin Fu**: Investigation; Data Curation
- **Junyue Zhang**: Data Curation; Writing - Original Draft
- **Zhiping Tao**: Supervision
- **Mengyuan Wang**: Writing - Review & Editing
- **Chong-Wen Zhou**: Supervision; Writing - Review & Editing; Project administration

Conflicts of interest

There are no conflicts to declare.

Acknowledgments

This work is supported by National Energy R&D Center of Petroleum Refining Technology (RIPP, SINOPEC) and the National Natural Science Foundation of China (Grant No. W2411043). Jingwu Sun is supported by a China Scholarship Council scholarship (202206020006), and this research was supported by the High Performance Computing Center of Beihang University.

Data availability

The supporting data has been provided as part of the Supplementary information. References cited in the Supplementary Information (SI) have been listed in the article's reference list.

References

1. E. Dzib, G. Merino, The hindered rotor theory: A review, *Wiley Interdiscip. Rev. Comput. Mol. Sci.*, 2022, **12**, e1583.
2. J. Zheng, T. Yu, E. Papajak, I. Alecu, S.L. Mielke, D.G. Truhlar, Practical methods for including torsional anharmonicity in thermochemical calculations on complex molecules: The internal-coordinate multi-structural approximation, *Phys. Chem. Chem. Phys.*, 2011, **13**, 10885-10907.
3. J. Zheng, D.G. Truhlar, Quantum thermochemistry: Multistructural method with torsional anharmonicity based on a coupled torsional potential, *J. Chem. Theory Comput.*, 2013, **9**, 1356-1367.
4. A. Valera-Medina, H. Xiao, M. Owen-Jones, W.I. David, P. Bowen, Ammonia for power, *Prog. Energy Combust. Sci.*, 2018, **69**, 63-102.
5. H. Stančin, H. Mikulčić, X. Wang, N. Duić, A review on alternative fuels in future energy system, *Renew. Sust. Energ. Rev.*, 2020, **128**, 109927.
6. L. Kang, W. Pan, J. Zhang, W. Wang, C. Tang, A review on ammonia blends combustion for industrial applications, *Fuel*, 2023, **332**, 126150.
7. X. Xu, E. Liu, N. Zhu, F. Liu, F. Qian, Review of the current status of ammonia-blended hydrogen fuel engine development, *Energies*, 2022, **15**, 1023.
8. L. Dai, S. Gersen, P. Glarborg, A. Mokhov, H. Levinsky, Autoignition studies of NH3/CH4 mixtures at high pressure, *Combust. Flame*, 2020, **218**, 19-26.
9. B. Wang, S. Dong, Z. Jiang, W. Gao, Z. Wang, J. Li, C. Yang, Z. Wang, X. Cheng, Development of a reduced chemical mechanism for ammonia/n-heptane blends, *Fuel*, 2023, **338**, 127358.
10. D. Wang, Z. Wang, T. Zhang, Y. Zhai, R. Hou, Z.-Y. Tian, C. Ji, A comparative study on the laminar C1–C4 n-alkane/NH_3 premixed flame, *Fuel*, 2022, **324**, 124732.
11. D. Zhu, B. Shu, Recent progress on combustion characteristics of ammonia-based fuel blends and their potential in internal combustion engines, *International Journal of Automotive Manufacturing and Materials*, 2023, **2**, 1.
12. M. Lubrano Lavadera, X. Han, A.A. Konnov, Comparative effect of ammonia addition on the laminar burning velocities of methane, n-heptane, and iso-octane, *Energy. Fuel.*, 2020, **35**, 7156-7168.
13. B.G. Harvey, H.A. Meylemans, The role of butanol in the development of sustainable fuel technologies, *J. Chem. Technol. Biot.*, 2011, **86**, 2-9.
14. C. Xue, X.-Q. Zhao, C.-G. Liu, L.-J. Chen, F.-W. Bai, Prospective and development of butanol as an advanced biofuel, *Biotechnol. Adv.*, 2013, **31**, 1575-1584.
15. W. Trindade, N-butanol as Biofuel Characteristics and Evaluation of its Application in Internal Combustion

View Article Online
DOI: 10.1039/D5CP04721H

Open Access Article. Published on 02 June 2026. Downloaded on 6/3/2026 5:39:24 AM.
This article is licensed under a Creative Commons Attribution 3.0 Unported Licence.

Engines through 1D Simulation, Master Thesis, Universidade Estadual de Campinas, 2016.
16. W. Zhong, L. Dai, Z. He, Q. Wang, Numerical study on the combustion characteristics of premixed ammonia flames with methanol/ethanol/n-butanol addition, *Fuel*, 2025, **381**, 13357.
17. G. Rees, T.C. Gray, Methyl-n-propyl ether, *Br. J. Anaesth.*, 1950, **22**, 83-91.
18. M.S. Johnson, M.R. Nimlos, E. Ninnemann, A. Laich, G.M. Fioroni, D. Kang, L. Bu, D. Ranasinghe, S. Khanniche, S.S. Goldsborough, Oxidation and pyrolysis of methyl propyl ether, *Int. J. Chem. Kinet.*, 2021, **53**, 915-938.
19. A. Çakmak, M. Kapusuz, H. Özcan, Experimental research on ethyl acetate as novel oxygenated fuel in the spark-ignition (SI) engine, *Energy Sources, Part A: Recovery, Utilization, and Environmental Effects*, 2023, **45**, 178-193.
20. S. Zhang, F. Guo, W. Yan, W. Dong, J. Zhou, W. Zhang, F. Xin, M. Jiang, Perspectives for the microbial production of ethyl acetate, *Appl. Microbiol. Biotechnol.*, 2020, **104**, 7239-7245.
21. S. Dong, B. Wang, Z. Jiang, Y. Li, W. Gao, Z. Wang, X. Cheng, H.J. Curran, An experimental and kinetic modeling study of ammonia/n-heptane blends, *Combust. Flame*, 2022, **246**, 112428.
22. M. Li, X. He, H. Hashemi, P. Glarborg, V.M. Lowe, P. Marshall, R. Fernandes, B. Shu, An experimental and modeling study on auto-ignition kinetics of ammonia/methanol mixtures at intermediate temperature and high pressure, *Combust. Flame*, 2022, **242**, 112160.
23. G. Issayev, B.R. Giri, A.M. Elbaz, K.P. Shrestha, F. Mauss, W.L. Roberts, A. Farooq, Ignition delay time and laminar flame speed measurements of ammonia blended with dimethyl ether: a promising low carbon fuel blend, *Renew. Energy*, 2022, **181**, 1353-1370.
24. J. Sun, Z. Fu, H. Zhu, Z. Tao, D. Wen, C.-W. Zhou, Theoretical kinetic study of key reactions between ammonia and fuel molecules, part I: Hydrogen atom abstraction from alkanes by $\dot{N}H_2$ radical, *Combust. Flame*, 2024, **261**, 113264.
25. Y. Tang, H.-H. Lu, J. Sun, Z. Fu, Z. Tao, L. Yang, C.-W. Zhou, Theoretical kinetics study of key reactions between ammonia and fuel molecules, part II: H-atom abstraction from alcohols and ethers by $\dot{N}H_2$ radicals, *Combust. Flame*, 2025, **271**, 113682.
26. J. Sun, L. Yang, D. Wen, H.J. Curran, C.-W. Zhou, A theoretical and kinetic study of key reactions between ammonia and fuel molecules, part III: H-atom abstraction from esters by $\dot{N}H_2$ radicals, *Combust. Flame*, 2024, **270**, 113738.
27. K.J. Laidler, M.C. King, The development of transition-state theory, *J. Phys. Chem.*, 1983, **87**, 2657-2664.
28. Y. Zhao, D.G. Truhlar, The M06 suite of density functionals for main group thermochemistry, thermochemical kinetics, noncovalent interactions, excited states, and transition elements: two new functionals and systematic testing of four M06-class functionals and 12 other functionals, *Theor. Chem. Acc.*, 2008, **120**, 215-241.
29. A. McLean, G. Chandler, Contracted Gaussian basis sets for molecular calculations. I. Second row atoms, Z= 11–18, *J. Chem. Phys.*, 1980, **72**, 5639-5648.
30. W.J. Hehre, R. Ditchfield, J.A. Pople, Self—consistent molecular orbital methods. XII. Further extensions of Gaussian—type basis sets for use in molecular orbital studies of organic molecules, *J. Chem. Phys.*, 1972, **56**, 2257-2261.
31. I.M. Alecu, J. Zheng, Y. Zhao, D.G. Truhlar, Computational thermochemistry: scale factor databases and scale factors for vibrational frequencies obtained from electronic model chemistries, *J. Chem. Theory Comput.*, 2010, **6**, 2872-2887.
32. M.e. Frisch, G. Trucks, H.B. Schlegel, G. Scuseria, M. Robb, J. Cheeseman, G. Scalmani, V. Barone, G. Petersson, H. Nakatsuji, Gaussian 16, Gaussian, Inc. Wallingford, CT, 2016.
33. J. Zheng, S.L. Mielke, K.L. Clarkson, D.G. Truhlar, MSTor: A program for calculating partition functions, free energies, enthalpies, entropies, and heat capacities of complex molecules including torsional anharmonicity, *Comput. Phys. Commun.*, 2012, **183**, 1803-1812.
34. W. Chen, J. Zheng, J.L. Bao, D.G. Truhlar, X. Xu, MSTor 2023: A new version of the computer code for multistructural torsional anharmonicity, now with automatic torsional identification using redundant internal coordinates, *Comput. Phys. Commun.*, 2023, **288**, 108740.
35. J.A. Montgomery Jr, M.J. Frisch, J.W. Ochterski, G.A. Petersson, A complete basis set model chemistry. VII. Use of the minimum population localization method, *J. Chem. Phys.*, 2000, **112**, 6532-6542.
36. J.W. Ochterski, G.A. Petersson, J.A. Montgomery Jr, A complete basis set model chemistry. V. Extensions to six or more heavy atoms, *J. Chem. Phys.*, 1996, **104**, 2598-2619.
37. L.A. Curtiss, K. Raghavachari, P.C. Redfern, V. Rassolov, J.A. Pople, Gaussian-3 (G3) theory for molecules containing first and second-row atoms, *J. Chem. Phys.*, 1998, **109**, 7764-7776.
38. L.A. Curtiss, P.C. Redfern, K. Raghavachari, Gaussian-4 theory, *J. Chem. Phys.*, 2007, **126**, 084108.
39. M. Keçeli, S.N. Elliott, Y.-P. Li, M.S. Johnson, C. Cavallotti, Y. Georgievskii, W.H. Green, M. Pelucchi, J.M. Wozniak, A.W. Jasper, Automated computational thermochemistry for butane oxidation: A prelude to predictive automated combustion kinetics, *Proc. Combust. Inst.*, 2019, **37**, 363-371.
40. P. Glarborg, J.A. Miller, B. Ruscic, S.J. Klippenstein, Modeling nitrogen chemistry in combustion, *Prog. Energy Combust. Sci.*, 2018, **67**, 31-68.

Physical Chemistry Chemical Physics Accepted Manuscript

View Article Online
DOI: 10.1039/D5CP04721H

Open Access Article. Published on 02 June 2026. Downloaded on 6/3/2026 5:39:24 AM.
This article is licensed under a Creative Commons Attribution 3.0 Unported Licence.

41. B.J. McBride, Computer program for calculating and fitting thermodynamic functions, National Aeronautics and Space Administration, Office of Management, 1992.
42. T. He, S. Li, Y. Chi, H.-B. Zhang, Z. Wang, B. Yang, X. He, X. You, An adaptive distance-based group contribution method for thermodynamic property prediction, *Phys. Chem. Chem. Phys.*, 2016, **18**, 23822-23830.
43. Y.P. Liu, G.C. Lynch, T.N. Truong, D.H. Lu, D.G. Truhlar, B.C. Garrett, Molecular modeling of the kinetic isotope effect for the [1, 5]-sigmatropic rearrangement of cis-1, 3-pentadiene, *J. Am. Chem. Soc.*, 1993, **115**, 2408-2415.
44. D.G. Truhlar, B.C. Garrett, Variational transition-state theory, *Acc. Chem. Res.*, 1980, **13**, 440-448.
45. J. Zheng, J. L. Bao, R. Meana-Pañeda, S. Zhang, B. J. Lynch, J. C. Corchado, Y.-Y. Chuang, P. L. Fast, W.-P. Hu, Y.-P. Liu, G. C. Lynch, K. A. Nguyen, C. F. Jackels, A. Fernandez Ramos, B. A. Ellingson, V. S. Melissas, J. Villà, I. Rossi, E. L. Coitiño, J. Pu, T. V. Albu, A. Ratkiewicz, R. Steckler, B. C. Garrett, A. D. Isaacson, and D. G. Truhlar Polyrate–version 2017, University of Minnesota, Minneapolis, 2018.
46. J. Zheng, J. Bao, S. Zhang, J. Corchado, R. Meana-Pañeda, Y. Chuang, E. Coitiño, B. Ellingson, D. Truhlar, Gaussrate 17, University of Minnesota: Minneapolis, MN, 2017.
47. A. González-Lafont, J. Villa, J.M. Lluch, J. Bertrán, R. Steckler, D.G. Truhlar, Variational transition state theory and tunneling calculations with reorientation of the generalized transition states for methyl cation transfer, *J. Phys. Chem. A*, 1998, **102**, 3420-3428.
48. T. Yu, J. Zheng, D.G. Truhlar, Statistical thermodynamics of the isomerization reaction between n-heptane and isoheptane, *Phys. Chem. Chem. Phys.*, 2012, **14**, 482-494.
49. Y. Gao, T. He, X. Li, X. You, Effect of hindered internal rotation treatments on predicting the thermodynamic properties of alkanes, *Phys. Chem. Chem. Phys.*, 2019, **21**, 1928-1936.
50. A. Burcat, B. Ruscic, Third millenium ideal gas and condensed phase thermochemical database for combustion (with update from active thermochemical tables), Argonne National Lab.(ANL), Argonne, IL (United States), 2005.
51. L. Dai, H. Hashemi, P. Glarborg, S. Gersen, P. Marshall, A. Mokhov, H. Levinsky, Ignition delay times of NH3/DME blends at high pressure and low DME fraction: RCM experiments and simulations, *Combust. Flame*, 2021, **227**, 120-134.
52. M.W. Chase Jr, N.-J.T. Tables, Data reported in NIST standard reference database 69, June 2005 release: NIST Chemistry WebBook, *J. Phys. Chem. Ref. Data*, 1998, **9**, 1-1951.
53. D. Pittam, G. Pilcher, Measurements of heats of combustion by flame calorimetry. Part 8.—Methane, ethane, propane, n-butane and 2-methylpropane, Journal of the Chemical Society, *Faraday Transactions 1: Physical Chemistry in Condensed Phases*, 1972, **68**, 2224-2229.
54. E.J. Prosen, F.D. Rossini, Heats of formation and combustion of 1, 3-butadiene and styrene, *Res. Nat. Bur. Stand*, 1945, **34**, 59.
55. B. Ruscic, D. Bross, Active Thermochemical Tables (ATcT) Values Based on ver. 1.122 q of the Thermochemical Network; Argonne National Laboratory: Lemont, IL, USA, 2021, available at ATcT. anl. gov, 2023.
56. W. Good, The enthalpies of combustion and formation of the isomeric pentanes, *J. Chem. Thermodyn.*, 1970, **2**, 237-244.
57. G. Pilcher, J. Chadwick, Measurements of heats of combustion by flame calorimetry. Part 4.—n-Pentane, isopentane, neopentane, *Trans. Faraday Soc.*, 1967, **63**, 2357-2361.
58. G. Messerly, R. Kennedy, The heat capacity and entropy, heats of fusion and vaporization and the vapor pressure of n-pentane, *J. Am. Chem. Soc.*, 1940, **62**, 2988-2991.
59. A.T.T.B.R.A.N.L. https://atct.anl.gov/.
60. A.B.a.B.R. Elke Goos, Extended Third Millenium Ideal Gas Thermochemical Database with updates from Active Thermochemical Tables. <http://burcat.technion.ac.il/dir>; 31 December 2019.
61. E. Prosen, K. Pitzer, F. Rossini, Heats and free energies of formation of the paraffin hydrocarbons, in the gaseous state, to 1500 degree K, *J. Res. Natl. Bur. Stand*, 1945, **34**, 403.
62. G.F. Davies, E. Gilbert, Heats of Combustion and of Formation of the Nine Isomeric Heptanes in the Liquid State, *J. Am. Chem. Soc.*, 1941, **63**, 2730-2732.
63. M. Chase, Data reported in NIST standard reference database 69, June 2005 release: NIST Chemistry WebBook, *J. Phys. Chem. Ref. Data*, 1998, **9**, 1.
64. J. Chao, K.R. Hall, K.N. Marsh, R.C. Wilhoit, Thermodynamic properties of key organic oxygen compounds in the carbon range C1 to C4. Part 2. Ideal gas properties, *J. Phys. Chem. Ref. Data*, **15**, 1369-1436.
65. M.E. Butwill, J.D. Rockenfeller, Heats of combustion and formation of ethyl acetate and isopropyl acetate, *Thermochim. Acta*, 1970, **1**, 289-295.
66. K.B. Wiberg, R.F. Waldron, Lactones. 2. Enthalpies of hydrolysis, reduction, and formation of the C4-C13 monocyclic lactones. Strain energies and conformations, *J. Am. Chem. Soc.*, 1991, **113**, 7697-7705.
67. J. Fenwick, D. Harrop, A. Head, Thermodynamic properties of organic oxygen compounds 46. Enthalpies of formation of ethyl acetate and 1-hexanoic acid, *J. Chem. Thermodyn.*, 1978, **10**, 687-690.

Physical Chemistry Chemical Physics Accepted Manuscript

View Article Online
DOI: 10.1039/D5CP04721H

68. K.B. Wiberg, L.S. Crocker, K.M. Morgan, Thermochemical studies of carbonyl compounds. 5. Enthalpies of reduction of carbonyl groups, *J. Am. Chem. Soc.*, 1991, **113**, 3447-3450.
69. D.R. Stull, E.F. Westrum, G.C. Sinke, The chemical thermodynamics of organic compounds, *J. Chem. Educ.*, 1970, **47**, 4.
70. J. Fenwick, D. Harrop, A. Head, Thermodynamic properties of organic oxygen compounds 41. Enthalpies of formation of eight ethers, *J. Chem. Thermodyn.*, 1975, **7**, 943-954.
71. G. Pilcher, A. Pell, D. Coleman, Measurements of heats of combustion by flame calorimetry. Part 2.—Dimethyl ether, methyl ethyl ether, methyl n-propyl ether, methyl isopropyl ether, *Trans. Faraday Soc.*, 1964, **60**, 499-505.
72. R. Andon, J. Martin, Thermodynamic properties of organic oxygen compounds 40. Heat capacity and entropy of six ethers, *J. Chem. Thermodyn.*, 1975, **7**, 593-606.
73. K. Siddique, M. Altarawneh, J. Gore, P.R. Westmoreland, B.Z. Dlugogorski, Hydrogen abstraction from hydrocarbons by $\dot{N}H_2$, *J. Phys. Chem. A*, 2017, **121**, 2221-2231.
74. A. Mebel, M. Lin, Prediction of absolute rate constants for the reactions of $\dot{N}H_2$ with alkanes from ab initio G2M/TST calculations, *J. Phys. Chem. A*, 1999, **103**, 2088-2096.
75. AutoMech program suite[CP/OL], https://github.com/Auto-Mech/MESS, 2024.
76. S. Chen, R.C. Wilhoit, B.J. Zwolinski, Ideal gas thermodynamic properties and isomerization of n-butane and isobutane, *J. Phys. Chem. Ref. Data*, 1975, **4**, 859-870.
77. D.W. Scott, Chemical Thermodynamic Properties of Hydrocarbons and Related Substances: Properties of the Alkane Hydrocarbons, C1 through C10, in the Ideal Gas State From 0 to 1500 K, US Department of the Interior, Bureau of Mines, 1974.

Open Access Article. Published on 02 June 2026. Downloaded on 6/3/2026 5:39:24 AM.
This article is licensed under a Creative Commons Attribution 3.0 Unported Licence.

Physical Chemistry Chemical Physics Accepted Manuscript

View Article Online
DOI: 10.1039/D5CP04721H

Data Availability Statement:

The authors confirm that the calculated data supporting the findings of this study are available within the article and its supplementary materials.

Open Access Article. Published on 02 June 2026. Downloaded on 6/3/2026 5:39:24 AM.
This article is licensed under a Creative Commons Attribution 3.0 Unported Licence.

Physical Chemistry Chemical Physics Accepted Manuscript